

Measurement of the ratio of branching fractions $\mathcal{B}(B^\pm \rightarrow J/\psi \pi^\pm)/\mathcal{B}(B^\pm \rightarrow J/\psi K^\pm)$

A. Abulencia,²⁴ J. Adelman,¹³ T. Affolder,¹⁰ T. Akimoto,⁵⁶ M. G. Albrow,¹⁷ D. Ambrose,¹⁷ S. Amerio,⁴⁴ D. Amidei,³⁵ A. Anastassov,⁵³ K. Anikeev,¹⁷ A. Annovi,¹⁹ J. Antos,¹⁴ M. Aoki,⁵⁶ G. Apollinari,¹⁷ J.-F. Arguin,³⁴ T. Arisawa,⁵⁸ A. Artikov,¹⁵ W. Ashmanskas,¹⁷ A. Attal,⁸ F. Azfar,⁴³ P. Azzi-Bacchetta,⁴⁴ P. Azzurri,⁴⁷ N. Bacchetta,⁴⁴ W. Badgett,¹⁷ A. Barbaro-Galtieri,²⁹ V. E. Barnes,⁴⁹ B. A. Barnett,²⁵ S. Baroiant,⁷ V. Bartsch,³¹ G. Bauer,³³ F. Bedeschi,⁴⁷ S. Behari,²⁵ S. Belforte,⁵⁵ G. Bellettini,⁴⁷ J. Bellinger,⁶⁰ A. Belloni,³³ D. Benjamin,¹⁶ A. Beretvas,¹⁷ J. Beringer,²⁹ T. Berry,³⁰ A. Bhatti,⁵¹ M. Binkley,¹⁷ D. Bisello,⁴⁴ R. E. Blair,² C. Blocker,⁶ B. Blumenfeld,²⁵ A. Bocci,¹⁶ A. Bodek,⁵⁰ V. Boisvert,⁵⁰ G. Bolla,⁴⁹ A. Bolshov,³³ D. Bortoletto,⁴⁹ J. Boudreau,⁴⁸ A. Boveia,¹⁰ B. Brau,¹⁰ L. Brigliadori,⁵ C. Bromberg,³⁶ E. Brubaker,¹³ J. Budagov,¹⁵ H. S. Budd,⁵⁰ S. Budd,²⁴ S. Budroni,⁴⁷ K. Burkett,¹⁷ G. Busetto,⁴⁴ P. Bussey,²¹ K. L. Byrum,² S. Cabrera,^{16,o} M. Campanelli,²⁰ M. Campbell,³⁵ F. Canelli,¹⁷ A. Canepa,⁴⁹ S. Carillo,^{18,i} D. Carlsmith,⁶⁰ R. Carosi,⁴⁷ S. Carron,³⁴ M. Casarsa,⁵⁵ A. Castro,⁵ P. Catastini,⁴⁷ D. Cauz,⁵⁵ M. Cavalli-Sforza,³ A. Cerri,²⁹ L. Cerrito,^{43,m} S. H. Chang,²⁸ Y. C. Chen,¹ M. Chertok,⁷ G. Chiarelli,⁴⁷ G. Chlachidze,¹⁵ F. Chlebana,¹⁷ I. Cho,²⁸ K. Cho,²⁸ D. Chokheli,¹⁵ J. P. Chou,²² G. Choudalakis,³³ S. H. Chuang,⁶⁰ K. Chung,¹² W. H. Chung,⁶⁰ Y. S. Chung,⁵⁰ M. Ciljak,⁴⁷ C. I. Ciobanu,²⁴ M. A. Ciocci,⁴⁷ A. Clark,²⁰ D. Clark,⁶ M. Coca,¹⁶ G. Compostella,⁴⁴ M. E. Convery,⁵¹ J. Conway,⁷ B. Cooper,³⁶ K. Copic,³⁵ M. Cordelli,¹⁹ G. Cortiana,⁴⁴ F. Crescioli,⁴⁷ C. Cuenca Almenar,^{7,o} J. Cuevas,^{11,j} R. Culbertson,¹⁷ J. C. Cully,³⁵ D. Cyr,⁶⁰ S. DaRonce,⁴⁴ M. Datta,¹⁷ S. D'Auria,²¹ T. Davies,²¹ M. D'Onofrio,³ D. Dagenhart,⁶ P. de Barbaro,⁵⁰ S. De Cecco,⁵² A. Deisher,²⁹ G. De Lentdecker,^{50,c} M. Dell'Orso,⁴⁷ F. Delli Paoli,⁴⁴ L. Demortier,⁵¹ J. Deng,¹⁶ M. Deninno,⁵ D. De Pedis,⁵² P. F. Derwent,¹⁷ G. P. Di Giovanni,⁴⁵ C. Dionisi,⁵² B. Di Ruzza,⁵⁵ J. R. Dittmann,⁴ P. DiTuro,⁵³ C. Dörr,²⁶ S. Donati,⁴⁷ M. Donega,²⁰ P. Dong,⁸ J. Donini,⁴⁴ T. Dorigo,⁴⁴ S. Dube,⁵³ J. Efron,⁴⁰ R. Erbacher,⁷ D. Errede,²⁴ S. Errede,²⁴ R. Eusebi,¹⁷ H. C. Fang,²⁹ S. Farrington,³⁰ I. Fedorko,⁴⁷ W. T. Fedorko,¹³ R. G. Feild,⁶¹ M. Feindt,²⁶ J. P. Fernandez,³² R. Field,¹⁸ G. Flanagan,⁴⁹ A. Foland,²² S. Forrester,⁷ G. W. Foster,¹⁷ M. Franklin,²² J. C. Freeman,²⁹ I. Furic,¹³ M. Gallinaro,⁵¹ J. Galyardt,¹² J. E. Garcia,⁴⁷ F. Garbersson,¹⁰ A. F. Garfinkel,⁴⁹ C. Gay,⁶¹ H. Gerberich,²⁴ D. Gerdes,³⁵ S. Giagu,⁵² P. Giannetti,⁴⁷ A. Gibson,²⁹ K. Gibson,⁴⁸ J. L. Gimmell,⁵⁰ C. Ginsburg,¹⁷ N. Giokaris,^{15,a} M. Giordani,⁵⁵ P. Giromini,¹⁹ M. Giunta,⁴⁷ G. Giurgiu,¹² V. Glagolev,¹⁵ D. Glenzinski,¹⁷ M. Gold,³⁸ N. Goldschmidt,¹⁸ J. Goldstein,^{43,b} A. Golossanov,¹⁷ G. Gomez,¹¹ G. Gomez-Ceballos,¹¹ M. Goncharov,⁵⁴ O. González,³² I. Gorelov,³⁸ A. T. Goshaw,¹⁶ K. Goulianos,⁵¹ A. Gresele,⁴⁴ M. Griffiths,³⁰ S. Grinstein,²² C. Grosso-Pilcher,¹³ R. C. Group,¹⁸ U. Grundler,²⁴ J. Guimaraes da Costa,²² Z. Gunay-Unalan,³⁶ C. Haber,²⁹ K. Hahn,³³ S. R. Hahn,¹⁷ E. Halkiadakis,⁵³ A. Hamilton,³⁴ B.-Y. Han,⁵⁰ J. Y. Han,⁵⁰ R. Handler,⁶⁰ F. Happacher,¹⁹ K. Hara,⁵⁶ M. Hare,⁵⁷ S. Harper,⁴³ R. F. Harr,⁵⁹ R. M. Harris,¹⁷ M. Hartz,⁴⁸ K. Hatakeyama,⁵¹ J. Hauser,⁸ A. Heijboer,⁴⁶ B. Heinemann,³⁰ J. Heinrich,⁴⁶ C. Henderson,³³ M. Herndon,⁶⁰ J. Heuser,²⁶ D. Hidas,¹⁶ C. S. Hill,^{10,b} D. Hirschbuehl,²⁶ A. Hocker,¹⁷ A. Holloway,²² S. Hou,¹ M. Houlden,³⁰ S.-C. Hsu,⁹ B. T. Huffman,⁴³ R. E. Hughes,⁴⁰ U. Husemann,⁶¹ J. Huston,³⁶ J. Incandela,¹⁰ G. Introzzi,⁴⁷ M. Iori,⁵² Y. Ishizawa,⁵⁶ A. Ivanov,⁷ B. Iyutin,³³ E. James,¹⁷ D. Jang,⁵³ B. Jayatilaka,³⁵ D. Jeans,⁵² H. Jensen,¹⁷ E. J. Jeon,²⁸ S. Jindariani,¹⁸ M. Jones,⁴⁹ K. K. Joo,²⁸ S. Y. Jun,¹² J. E. Jung,²⁸ T. R. Junk,²⁴ T. Kamon,⁵⁴ P. E. Karchin,⁵⁹ Y. Kato,⁴² Y. Kemp,²⁶ R. Kephart,¹⁷ U. Kerzel,²⁶ V. Khotilovich,⁵⁴ B. Kilminster,⁴⁰ D. H. Kim,²⁸ H. S. Kim,²⁸ J. E. Kim,²⁸ M. J. Kim,¹² S. B. Kim,²⁸ S. H. Kim,⁵⁶ Y. K. Kim,¹³ N. Kimura,⁵⁶ L. Kirsch,⁶ S. Klimenko,¹⁸ M. Klute,³³ B. Knuteson,³³ B. R. Ko,¹⁶ K. Kondo,⁵⁸ D. J. Kong,²⁸ J. Konigsberg,¹⁸ A. Korytov,¹⁸ A. V. Kotwal,¹⁶ A. Kovalev,⁴⁶ A. C. Kraan,⁴⁶ J. Kraus,²⁴ I. Kravchenko,³³ M. Kreps,²⁶ J. Kroll,⁴⁶ N. Krumnack,⁴ M. Kruse,¹⁶ V. Krutelyov,¹⁰ T. Kubo,⁵⁶ S. E. Kuhlmann,² T. Kuhr,²⁶ Y. Kusakabe,⁵⁸ S. Kwang,¹³ A. T. Laasanen,⁴⁹ S. Lai,³⁴ S. Lami,⁴⁷ S. Lammel,¹⁷ M. Lancaster,³¹ R. L. Lander,⁷ K. Lannon,⁴⁰ A. Lath,⁵³ G. Latino,⁴⁷ I. Lazzizzera,⁴⁴ T. LeCompte,² J. Lee,⁵⁰ J. Lee,²⁸ Y. J. Lee,²⁸ S. W. Lee,^{54,n} R. Lefèvre,³ N. Leonardo,³³ S. Leone,⁴⁷ S. Levy,¹³ J. D. Lewis,¹⁷ C. Lin,⁶¹ C. S. Lin,¹⁷ M. Lindgren,¹⁷ E. Lipeles,⁹ A. Lister,⁷ D. O. Litvintsev,¹⁷ T. Liu,¹⁷ N. S. Lockyer,⁴⁶ A. Loginov,⁶¹ M. Loretì,⁴⁴ P. Loverre,⁵² R.-S. Lu,¹ D. Lucchesi,⁴⁴ P. Lujan,²⁹ P. Lukens,¹⁷ G. Lungu,¹⁸ L. Lyons,⁴³ J. Lys,²⁹ R. Lysak,¹⁴ E. Lytken,⁴⁹ P. Mack,²⁶ D. MacQueen,³⁴ R. Madrak,¹⁷ K. Maeshima,¹⁷ K. Makhoul,³³ T. Maki,²³ P. Maksimovic,²⁵ S. Malde,⁴³ G. Manca,³⁰ F. Margaroli,⁵ R. Marginean,¹⁷ C. Marino,²⁶ C. P. Marino,²⁴ A. Martin,⁶¹ M. Martin,²¹ V. Martin,^{21,g} M. Martínez,³ T. Maruyama,⁵⁶ P. Mastrandrea,⁵² T. Masubuchi,⁵⁶ H. Matsunaga,⁵⁶ M. E. Mattson,⁵⁹ R. Mazini,³⁴ P. Mazzanti,⁵ K. S. McFarland,⁵⁰ P. McIntyre,⁵⁴ R. McNulty,^{30,f} A. Mehta,³⁰ P. Mehtala,²³ S. Menzemer,^{11,h} A. Menzione,⁴⁷ P. Merkel,⁴⁹ C. Mesropian,⁵¹ A. Messina,³⁶ T. Miao,¹⁷ N. Miladinovic,⁶ J. Miles,³³ R. Miller,³⁶ C. Mills,¹⁰ M. Milnik,²⁶ A. Mitra,¹ G. Mitselmakher,¹⁸ A. Miyamoto,²⁷ S. Moed,²⁰ N. Moggi,⁵ B. Mohr,⁸ R. Moore,¹⁷ M. Morello,⁴⁷ P. Movilla Fernandez,²⁹ J. Mülmenstädt,²⁹ A. Mukherjee,¹⁷ Th. Müller,²⁶ R. Mumford,²⁵ P. Murat,¹⁷ J. Nachtman,¹⁷ A. Nagano,⁵⁶ J. Naganoma,⁵⁸ I. Nakano,⁴¹ A. Napier,⁵⁷ V. Necula,¹⁸ C. Neu,⁴⁶ M. S. Neubauer,⁹ J. Nielsen,²⁹

T. Nigmanov,⁴⁸ L. Nodulman,² O. Norriella,³ E. Nurse,³¹ S. H. Oh,¹⁶ Y. D. Oh,²⁸ I. Oksuzian,¹⁸ T. Okusawa,⁴² R. Oldeman,³⁰ R. Orava,²³ K. Osterberg,²³ C. Pagliarone,⁴⁷ E. Palencia,¹¹ V. Papadimitriou,¹⁷ A. A. Paramonov,¹³ B. Parks,⁴⁰ S. Pashapour,³⁴ J. Patrick,¹⁷ G. Pauletta,⁵⁵ M. Paulini,¹² C. Paus,³³ D. E. Pellett,⁷ A. Penzo,⁵⁵ T. J. Phillips,¹⁶ G. Piacentino,⁴⁷ J. Piedra,⁴⁵ L. Pina,¹⁸ K. Pitts,²⁴ C. Plager,⁸ L. Pondrom,⁶⁰ X. Portell,³ O. Poukhov,¹⁵ N. Pounder,⁴³ F. Prakoshyn,¹⁵ A. Pronko,¹⁷ J. Proudfoot,² F. Ptohos,^{19,e} G. Punzi,⁴⁷ J. Pursley,²⁵ J. Rademacker,^{43,b} A. Rahaman,⁴⁸ N. Ranjan,⁴⁹ S. Rappoccio,²² B. Reiser,¹⁷ V. Rekovic,³⁸ P. Renton,⁴³ M. Rescigno,⁵² S. Richter,²⁶ F. Rimondi,⁵ L. Ristori,⁴⁷ A. Robson,²¹ T. Rodrigo,¹¹ E. Rogers,²⁴ S. Rolli,⁵⁷ R. Roser,¹⁷ M. Rossi,⁵⁵ R. Rossin,¹⁸ A. Ruiz,¹¹ J. Russ,¹² V. Rusu,¹³ H. Saarikko,²³ S. Sabik,³⁴ A. Safonov,⁵⁴ W. K. Sakumoto,⁵⁰ G. Salamanna,⁵² O. Saltó,³ D. Saltzberg,⁸ C. Sánchez,³ L. Santi,⁵⁵ S. Sarkar,⁵² L. Sartori,⁴⁷ K. Sato,¹⁷ P. Savard,³⁴ A. Savoy-Navarro,⁴⁵ T. Scheidle,²⁶ P. Schlabach,¹⁷ E. E. Schmidt,¹⁷ M. P. Schmidt,⁶¹ M. Schmitt,³⁹ T. Schwarz,⁷ L. Scodellaro,¹¹ A. L. Scott,¹⁰ A. Scribano,⁴⁷ F. Scuri,⁴⁷ A. Sedov,⁴⁹ S. Seidel,³⁸ Y. Seiya,⁴² A. Semenov,¹⁵ L. Sexton-Kennedy,¹⁷ A. Sfyrla,²⁰ M. D. Shapiro,²⁹ T. Shears,³⁰ P. F. Shepard,⁴⁸ D. Sherman,²² M. Shimojima,^{56,k} M. Shochet,¹³ Y. Shon,⁶⁰ I. Shreyber,³⁷ A. Sidoti,⁴⁷ P. Sinervo,³⁴ A. Sisakyan,¹⁵ J. Sjolin,⁴³ A. J. Slaughter,¹⁷ J. Slaunwhite,⁴⁰ K. Sliwa,⁵⁷ J. R. Smith,⁷ F. D. Snider,¹⁷ R. Snihur,³⁴ M. Soderberg,³⁵ A. Soha,⁷ S. Somalwar,⁵³ V. Sorin,³⁶ J. Spalding,¹⁷ F. Spinella,⁴⁷ T. Spreitzer,³⁴ P. Squillacioti,⁴⁷ M. Stanitzki,⁶¹ A. Staveris-Polykalas,⁴⁷ R. St. Denis,²¹ B. Stelzer,⁸ O. Stelzer-Chilton,⁴³ D. Stentz,³⁹ J. Strologas,³⁸ D. Stuart,¹⁰ J. S. Suh,²⁸ A. Sukhanov,¹⁸ H. Sun,⁵⁷ T. Suzuki,⁵⁶ A. Taffard,²⁴ R. Takashima,⁴¹ Y. Takeuchi,⁵⁶ K. Takikawa,⁵⁶ M. Tanaka,² R. Tanaka,⁴¹ M. Tecchio,³⁵ P. K. Teng,¹ K. Terashi,⁵¹ J. Thom,^{17,d} A. S. Thompson,²¹ E. Thomson,⁴⁶ P. Tipton,⁶¹ V. Tiwari,¹² S. Tkaczyk,¹⁷ D. Toback,⁵⁴ S. Tokar,¹⁴ K. Tollefson,³⁶ T. Tomura,⁵⁶ D. Tonelli,⁴⁷ S. Torre,¹⁹ D. Torretta,¹⁷ S. Tourneur,⁴⁵ W. Trischuk,³⁴ R. Tsuchiya,⁵⁸ S. Tsuno,⁴¹ N. Turini,⁴⁷ F. Ukegawa,⁵⁶ T. Unverhau,²¹ S. Uozumi,⁵⁶ D. Usynin,⁴⁶ S. Vallecorsa,²⁰ N. van Remortel,²³ A. Varganov,³⁵ E. Vataga,³⁸ F. Vázquez,^{18,i} G. Velev,¹⁷ G. Veramendi,²⁴ V. Veszpremi,⁴⁹ R. Vidal,¹⁷ I. Vila,¹¹ R. Vilar,¹¹ T. Vine,³¹ I. Vollrath,³⁴ I. Volobouev,^{29,n} G. Volpi,⁴⁷ F. Würthwein,⁹ P. Wagner,⁵⁴ R. G. Wagner,² R. L. Wagner,¹⁷ J. Wagner,²⁶ W. Wagner,²⁶ R. Wallny,⁸ S. M. Wang,¹ A. Warburton,³⁴ S. Waschke,²¹ D. Waters,³¹ M. Weinberger,⁵⁴ W. C. Wester III,¹⁷ B. Whitehouse,⁵⁷ D. Whiteson,⁴⁶ A. B. Wicklund,² E. Wicklund,¹⁷ G. Williams,³⁴ H. H. Williams,⁴⁶ P. Wilson,¹⁷ B. L. Winer,⁴⁰ P. Wittich,^{17,d} S. Wolbers,¹⁷ C. Wolfe,¹³ T. Wright,³⁵ X. Wu,²⁰ S. M. Wynne,³⁰ A. Yagil,¹⁷ K. Yamamoto,⁴² J. Yamaoka,⁵³ T. Yamashita,⁴¹ C. Yang,⁶¹ U. K. Yang,^{13,j} Y. C. Yang,²⁸ W. M. Yao,²⁹ G. P. Yeh,¹⁷ J. Yoh,¹⁷ K. Yorita,¹³ T. Yoshida,⁴² G. B. Yu,⁵⁰ I. Yu,²⁸ S. S. Yu,¹⁷ J. C. Yun,¹⁷ L. Zanello,⁵² A. Zanetti,⁵⁵ I. Zaw,²² X. Zhang,²⁴ J. Zhou,⁵³ and S. Zucchelli⁵

(CDF Collaboration)

¹*Institute of Physics, Academia Sinica, Taipei, Taiwan 11529, Republic of China*²*Argonne National Laboratory, Argonne, Illinois 60439, USA*³*Institut de Física d'Altes Energies, Universitat Autònoma de Barcelona, E-08193, Bellaterra (Barcelona), Spain*⁴*Baylor University, Waco, Texas 76798, USA*⁵*Istituto Nazionale di Fisica Nucleare, University of Bologna, I-40127 Bologna, Italy*⁶*Brandeis University, Waltham, Massachusetts 02254, USA*⁷*University of California, Davis, Davis, California 95616, USA*⁸*University of California, Los Angeles, Los Angeles, California 90024, USA*⁹*University of California, San Diego, La Jolla, California 92093, USA*¹⁰*University of California, Santa Barbara, Santa Barbara, California 93106, USA*¹¹*Instituto de Física de Cantabria, CSIC-University of Cantabria, 39005 Santander, Spain*¹²*Carnegie Mellon University, Pittsburgh, Pennsylvania 15213, USA*¹³*Enrico Fermi Institute, University of Chicago, Chicago, Illinois 60637, USA*¹⁴*Comenius University, 842 48 Bratislava, Slovakia; Institute of Experimental Physics, 040 01 Kosice, Slovakia*¹⁵*Joint Institute for Nuclear Research, RU-141980 Dubna, Russia*¹⁶*Duke University, Durham, North Carolina 27708, USA*¹⁷*Fermi National Accelerator Laboratory, Batavia, Illinois 60510, USA*¹⁸*University of Florida, Gainesville, Florida 32611, USA*¹⁹*Laboratori Nazionali di Frascati, Istituto Nazionale di Fisica Nucleare, I-00044 Frascati, Italy*²⁰*University of Geneva, CH-1211 Geneva 4, Switzerland*²¹*Glasgow University, Glasgow G12 8QQ, United Kingdom*²²*Harvard University, Cambridge, Massachusetts 02138, USA*²³*Division of High Energy Physics, Department of Physics, University of Helsinki and Helsinki Institute of Physics, FIN-00014, Helsinki, Finland*²⁴*University of Illinois, Urbana, Illinois 61801, USA*

- ²⁵The Johns Hopkins University, Baltimore, Maryland 21218, USA
²⁶Institut für Experimentelle Kernphysik, Universität Karlsruhe, 76128 Karlsruhe, Germany
²⁷High Energy Accelerator Research Organization (KEK), Tsukuba, Ibaraki 305, Japan
²⁸Center for High Energy Physics: Kyungpook National University, Taegu 702-701, Korea; Seoul National University, Seoul 151-742, Korea; and SungKyunKwan University, Suwon 440-746, Korea
²⁹Ernest Orlando Lawrence Berkeley National Laboratory, Berkeley, California 94720, USA
³⁰University of Liverpool, Liverpool L69 7ZE, United Kingdom
³¹University College London, London WC1E 6BT, United Kingdom
³²Centro de Investigaciones Energeticas Medioambientales y Tecnologicas, E-28040 Madrid, Spain
³³Massachusetts Institute of Technology, Cambridge, Massachusetts 02139, USA
³⁴Institute of Particle Physics: McGill University, Montréal, Canada H3A 2T8; and University of Toronto, Toronto, Canada M5S 1A7
³⁵University of Michigan, Ann Arbor, Michigan 48109, USA
³⁶Michigan State University, East Lansing, Michigan 48824, USA
³⁷Institution for Theoretical and Experimental Physics, ITEP, Moscow 117259, Russia
³⁸University of New Mexico, Albuquerque, New Mexico 87131, USA
³⁹Northwestern University, Evanston, Illinois 60208, USA
⁴⁰The Ohio State University, Columbus, Ohio 43210, USA
⁴¹Okayama University, Okayama 700-8530, Japan
⁴²Osaka City University, Osaka 588, Japan
⁴³University of Oxford, Oxford OX1 3RH, United Kingdom
⁴⁴University of Padova, Istituto Nazionale di Fisica Nucleare, Sezione di Padova-Trento, I-35131 Padova, Italy
⁴⁵LPNHE, Université Pierre et Marie Curie/IN2P3-CNRS, UMR7585, Paris, F-75252 France
⁴⁶University of Pennsylvania, Philadelphia, Pennsylvania 19104, USA
⁴⁷Istituto Nazionale di Fisica Nucleare Pisa, Universities of Pisa, Siena, and Scuola Normale Superiore, I-56127 Pisa, Italy
⁴⁸University of Pittsburgh, Pittsburgh, Pennsylvania 15260, USA
⁴⁹Purdue University, West Lafayette, Indiana 47907, USA
⁵⁰University of Rochester, Rochester, New York 14627, USA
⁵¹The Rockefeller University, New York, New York 10021, USA
⁵²Istituto Nazionale di Fisica Nucleare, Sezione di Roma 1, University of Rome “La Sapienza”, I-00185 Roma, Italy
⁵³Rutgers University, Piscataway, New Jersey 08855, USA
⁵⁴Texas A&M University, College Station, Texas 77843, USA
⁵⁵Istituto Nazionale di Fisica Nucleare, University of Trieste/Udine, Italy
⁵⁶University of Tsukuba, Tsukuba, Ibaraki 305, Japan
⁵⁷Tufts University, Medford, Massachusetts 02155, USA
⁵⁸Waseda University, Tokyo 169, Japan
⁵⁹Wayne State University, Detroit, Michigan 48201, USA
⁶⁰University of Wisconsin, Madison, Wisconsin 53706, USA
⁶¹Yale University, New Haven, Connecticut 06520, USA

(Received 25 January 2007; revised manuscript received 19 February 2009; published 10 June 2009)

We report a measurement of the ratio of branching fractions of the decays $B^\pm \rightarrow J/\psi \pi^\pm$ and $B^\pm \rightarrow J/\psi K^\pm$ using the CDF II detector at the Fermilab Tevatron Collider. The signal from the Cabibbo-suppressed $B^\pm \rightarrow J/\psi \pi^\pm$ decay is separated from $B^\pm \rightarrow J/\psi K^\pm$ using the $B^\pm \rightarrow J/\psi K^\pm$ invariant mass distribution and the kinematical differences of the hadron track in the two decay modes. From a sample of 220 pb^{-1} of $p\bar{p}$ collisions at $\sqrt{s} = 1.96 \text{ TeV}$, we observe $91 \pm 15 B^\pm \rightarrow J/\psi \pi^\pm$ events together with $1883 \pm 34 B^\pm \rightarrow J/\psi K^\pm$ events. The ratio of branching fractions is found to be $\mathcal{B}(B^\pm \rightarrow J/\psi \pi^\pm)/\mathcal{B}(B^\pm \rightarrow J/\psi K^\pm) = (4.86 \pm 0.82(\text{stat}) \pm 0.15(\text{sys}))\%$.

DOI: 10.1103/PhysRevD.79.112003

PACS numbers: 13.25.Hw, 14.40.Nd

^aVisiting from University of Athens.

^bVisiting from University of Bristol.

^cVisiting from University Libre de Bruxelles.

^dVisiting from Cornell University.

^eVisiting from University of Cyprus.

^fVisiting from University of Dublin.

^gVisiting from University of Edinburgh.

^hVisiting from University of Heidelberg.

ⁱVisiting from Universidad Iberoamericana.

^jVisiting from University of Manchester.

^kVisiting from Nagasaki Institute of Applied Science.

^lVisiting from University de Oviedo.

^mVisiting from University of London, Queen Mary, and Westfield College.

ⁿVisiting from Texas Tech University.

^oVisiting from IFIC (CSIC-Universitat de Valencia).

The $B^\pm \rightarrow J/\psi \pi^\pm$ decay is a Cabibbo-suppressed mode proceeding via a $b \rightarrow c\bar{c}d$ transition. If the leading-order tree diagram is the dominant contribution, its branching fraction is expected to be $\approx 5\%$ of that of the Cabibbo-favored mode $B^\pm \rightarrow J/\psi K^\pm$. Detailed predictions of the ratio are obtained using the hypothesis of factorization of the hadronic matrix elements [1,2], a theoretical approach widely used in the treatment of nonleptonic decays of B mesons. However, the absence of strong theoretical arguments supporting factorization and the use of phenomenological models, which are a source of theoretical uncertainties, weaken the reliability of those predictions, which need to be accurately tested on data. Until now, the measurements on the $B^\pm \rightarrow J/\psi \pi^\pm$ decay were performed by many experiments. The BABAR collaboration reported $\mathcal{B}(B^\pm \rightarrow J/\psi \pi^\pm)/\mathcal{B}(B^\pm \rightarrow J/\psi K^\pm) = (5.37 \pm 0.45)\%$ with $244 \pm 20 B^\pm \rightarrow J/\psi \pi^\pm$ events [3]. The Belle collaboration reported $\mathcal{B}(B^\pm \rightarrow J/\psi \pi^\pm) = (3.8 \pm 0.6) \times 10^{-5}$ [4]. A previous study of the $B^\pm \rightarrow J/\psi \pi^\pm$ decay was also performed by the CLEO collaboration [5]. The result of this analysis supersedes the previous CDF result [6].

This paper presents a measurement of the ratio of branching fractions $\mathcal{B}(B^\pm \rightarrow J/\psi \pi^\pm)/\mathcal{B}(B^\pm \rightarrow J/\psi K^\pm)$. We use a sample of fully reconstructed $B^\pm \rightarrow J/\psi K^\pm$ decays, where $J/\psi \rightarrow \mu^+ \mu^-$, corresponding to an integrated luminosity of 220 pb^{-1} of $p\bar{p}$ collisions at $\sqrt{s} = 1.96 \text{ TeV}$ collected by the CDF II detector at Fermilab between February 2002 and August 2003.

The CDF II detector is a multipurpose detector [7] with a central geometry and has a tracking system surrounded by calorimeters and muon detectors. The components of the detector most relevant to this analysis are described briefly here. Charged particle trajectories are reconstructed in the pseudorapidity range $|\eta| < 1.0$, where $\eta = -\ln(\tan\frac{\theta}{2})$, and θ is the polar angle measured from the beam line [8]. Trajectories are reconstructed from hits in the silicon microstrip detector [9] and the central outer tracker (COT) [10] which are immersed in a 1.4 T solenoidal magnetic field. The silicon microstrip detector consists of five concentric layers made of double-sided silicon detectors with radii between 2.5 and 10.6 cm, each providing a position measurement with $15 \mu\text{m}$ resolution in the $r - \phi$ plane. The COT is an open-cell drift chamber with 96 measurement layers, between 40 and 137 cm in radius, organized into eight alternating axial and $\pm 2^\circ$ stereo superlayers. The transverse momentum (p_T) resolution is $\sigma_{p_T}/p_T \approx 0.15\% p_T (\text{GeV}/c)^{-1}$. Muon detectors consisting of multi-layer drift chambers are located radially around the outside of the calorimeter [11]. The central muon detector (CMU) covers a range in the pseudorapidity of $|\eta| < 0.6$. The central muon extension (CMX) extends the pseudorapidity coverage to $0.6 < |\eta| < 1.0$.

The data sample used in this analysis required a dimuon trigger sensitive to $J/\psi \rightarrow \mu^+ \mu^-$. The CDF II detector

employs a three-level trigger system to select events of interest efficiently. At the first trigger level, muon candidates are identified by matching track segments in the CMU and CMX to coarsely reconstructed COT tracks obtained with the extremely fast tracker [12]. Dimuon triggers use combinations of CMU-CMU and CMU-CMX muons with $p_T > 1.5(2.0) \text{ GeV}/c$ for CMU (CMX) muons. For the data presented here, no additional requirements are made at the second level. At the third trigger level, a detailed reconstruction is performed, and oppositely charged dimuon events with an invariant mass in the range of $2.7\text{--}4.0 \text{ GeV}/c^2$ are selected.

In this analysis, we reconstruct $B^\pm \rightarrow J/\psi K^\pm$ decays. B meson decay modes involving the well-known $J/\psi \rightarrow \mu^+ \mu^-$ decay have been extensively used in other measurements at CDF, and their selection criteria are well established. We follow the selection requirements developed in the b hadron mass measurement [13] and apply them to the B^\pm decay mode of interest. To ensure the best momentum scale calibration, the data sample used for this analysis is also kept the same as that for the mass measurement.

The $B^\pm \rightarrow J/\psi K^\pm$ reconstruction begins by selecting $J/\psi \rightarrow \mu^+ \mu^-$ candidates with pairs of oppositely charged tracks which satisfy the requirements of the dimuon triggers. J/ψ candidates are further selected by requiring their invariant mass to be within $80 \text{ MeV}/c^2$ of the world average J/ψ mass [14]. After a J/ψ candidate is identified, any other charged track is assumed to be a kaon and is combined with the J/ψ candidate to make a B^\pm candidate. The tracks of the kaon and two muons are then fitted to a common three dimensional vertex (3D) while constraining the invariant mass of two muons to the world average J/ψ mass [14]. To ensure good vertex resolution, each track must have hits in at least three silicon vertex detector layers in the $r - \phi$ plane and the probability resulting from the 3D vertex fit is required to be greater than 1%.

A number of further requirements are made to improve the signal-to-background separation. Prompt background, with tracks coming directly from the primary vertex, can be reduced by exploiting variables sensitive to the long lifetime of the B^\pm meson. To reduce prompt background, the transverse decay length (L_{xy}) of the B^\pm is required to exceed $200 \mu\text{m}$, where L_{xy} is defined as the vector from the primary vertex to the B^\pm decay vertex projected onto the p_T of the B^\pm candidate. To further reduce combinatorial background, we require $p_T > 6.5 \text{ GeV}/c$ for the B^\pm candidate and $p_T > 2.0 \text{ GeV}/c$ for the hadron from the B^\pm decay. The values used in the above selection criteria are determined by an iterative optimization procedure in which the significance $S/\sqrt{S+B}$ is maximized. The quantity S represents the number of accepted signal events, in this case taken from a Monte Carlo simulation sample, and B is the number of selected B^\pm candidates within the mass sidebands of the data.

We measure the following ratio:

$$\frac{\mathcal{B}(B^\pm \rightarrow J/\psi \pi^\pm)}{\mathcal{B}(B^\pm \rightarrow J/\psi K^\pm)} = \frac{N_{J/\psi \pi^\pm}}{N_{J/\psi K^\pm}} \times \frac{\epsilon_{J/\psi K^\pm}}{\epsilon_{J/\psi \pi^\pm}} = r_{\text{obs}} \times \frac{1}{\epsilon_{\text{rel}}}, \quad (1)$$

where $r_{\text{obs}} (\equiv N_{J/\psi \pi^\pm} / N_{J/\psi K^\pm})$ is the ratio of the yields of each decay mode, and $\epsilon_{\text{rel}} (\equiv \epsilon_{J/\psi \pi^\pm} / \epsilon_{J/\psi K^\pm})$ is the relative reconstruction efficiency. In this analysis, the quantity r_{obs} is extracted from an unbinned maximum likelihood fit using the differences between the two decay modes in the mass distribution and is corrected with ϵ_{rel} obtained from Monte Carlo simulation.

To build the probability density function (PDF) used in the unbinned maximum likelihood fit, we choose the invariant mass of J/ψ and a kaon ($M_{J/\psi K}$) as an observable. There are three components in the distribution of the $M_{J/\psi K}$ variable: the $B^\pm \rightarrow J/\psi K^\pm$ signal, the $B^\pm \rightarrow J/\psi \pi^\pm$ signal, and the combinatorial background. As demonstrated in the high statistics D and B mass reconstructions with similar decay topology, the invariant mass distribution of $B^\pm \rightarrow J/\psi K^\pm$ decay at CDF is well described by a Gaussian function with a width determined by CDF's tracking resolution [13,15,16]. Therefore, we model the $B^\pm \rightarrow J/\psi K^\pm$ signal as a Gaussian centered at the mass of B^\pm (M_B) with a width σ_K . If the pion mass were assigned to the hadron track originating from the $B^\pm \rightarrow J/\psi \pi^\pm$ decay, the resulting spectrum would also be a Gaussian centered at M_B . However, assigning the kaon mass to this track produces a spectrum partially overlapping the $B^\pm \rightarrow J/\psi K^\pm$ and shifted in the positive direction. The shifted invariant mass of $B^\pm \rightarrow J/\psi \pi^\pm$ can be calculated by an approximation, which has a good agreement with the exact value [17],

$$\mathcal{M}_B^{\prime 2}(\alpha) \simeq M_B^2 + (1 + \alpha)(M_K^2 - M_\pi^2), \quad (2)$$

where M_K and M_π are, respectively, the kaon and the pion masses. The purely kinematic variable α is defined as $\alpha \equiv E_{J/\psi} / P_K$, where $E_{J/\psi}$ is the J/ψ energy and P_K is the magnitude of the momentum of the hadron track. Using Eq. (2), the $B^\pm \rightarrow J/\psi \pi^\pm$ signal is modeled as a Gaussian centered at $\mathcal{M}_B^{\prime}(\alpha)$ with a width σ_π . We find σ_K and σ_π have almost the same value from the Monte Carlo simulation, so we constrain them to be the same value in the fit. We assume the background mass distribution is a first order polynomial. In the likelihood, we also include the PDF functions of α for $B^\pm \rightarrow J/\psi K^\pm$ and $B^\pm \rightarrow J/\psi \pi^\pm$ as the distributions for the two signals are found to be slightly different. We parametrize α PDF distributions from the Monte Carlo simulation. We also parametrize the α distribution of the background, which is obtained from the mass sidebands of the data. These mass sidebands are chosen from $5.2 < M_{J/\psi K} < 5.24$ and $5.4 < M_{J/\psi K} < 5.6$ GeV/c^2 to avoid signal contaminations and other backgrounds from partially reconstructed B mesons that

fall below 5.2 GeV/c^2 . The empirical functions used in the parametrizations are

$$h_{J/\psi X}(\alpha; f_i, \lambda_i, a) = \sum_{i=1}^3 f_i(\alpha - a)e^{-\lambda_i \alpha}, \quad (3)$$

$$h_{bkg}(\alpha; f_i, \lambda_i, a) = \sum_{i=1}^3 f_i(\alpha - a)^3 e^{-\lambda_i \alpha}, \quad (4)$$

where the symbol X denotes K or π in Eq. (3), and f_1, f_2 , and f_3 are to be the fractional contributions of each type of function when the functions are properly normalized to 1. Because of the requirement on the p_T of the hadron track and also of the dimuon triggers, all α distributions show a cutoff around 0.5 in the α variable, and these cutoff values are parametrized by a in Eqs. (3) and (4). These parameters of the functions describing the α distributions are fixed in the fit. The α distributions of the signal and background, and the results of the parameters are shown in Fig. 1. With models for each signal and background, and with the chosen observables, the PDF of the i th event is written as

$$p_i = f_s \left[\frac{1}{1 + r_{\text{obs}}} G(M_{J/\psi K}^i - M_B, \sigma) h_{J/\psi K}(\alpha^i) + \frac{r_{\text{obs}}}{1 + r_{\text{obs}}} G(M_{J/\psi K}^i - \mathcal{M}_B^{\prime}(\alpha^i), \sigma) h_{J/\psi \pi}(\alpha^i) \right] + (1 - f_s) B(M_{J/\psi K}^i) h_{bkg}(\alpha^i), \quad (5)$$

where f_s is the fraction of signal events in the data sample, and r_{obs} is the ratio between the yields of each signal. The functions, $G(M_{J/\psi K}^i - M_B, \sigma)$ and $G(M_{J/\psi K}^i - \mathcal{M}_B^{\prime}(\alpha^i), \sigma)$,

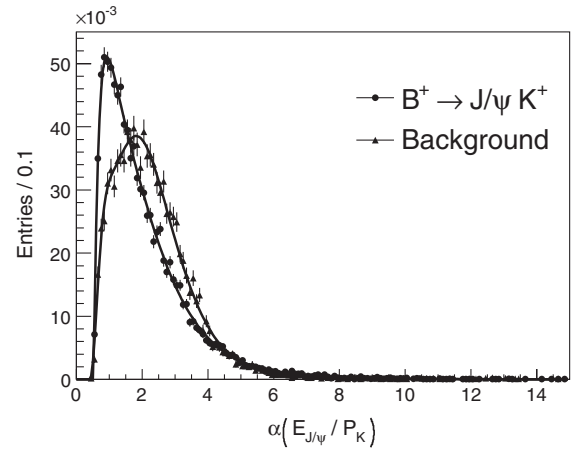


FIG. 1. The α distributions of $B^\pm \rightarrow J/\psi K^\pm$, which are obtained with Monte Carlo simulation and background obtained from the nonsignal data sample. The solid curves are the corresponding parametrization functions from Eqs. (3) and (4). The α distributions of the two signals are very similar in shape due to the almost identical kinematics of the two decay modes. To avoid confusion from it, we plot the α distribution of $B^\pm \rightarrow J/\psi K^\pm$ only.

are Gaussians with a width σ describing the mass distributions of $B^\pm \rightarrow J/\psi K^\pm$ and $B^\pm \rightarrow J/\psi \pi^\pm$, respectively, and $B(M_{J/\psi K}^i)$ is a first order polynomial function which describes the background mass distribution. The fitting range ($5.2 < M_{J/\psi K} < 5.6 \text{ GeV}/c^2$) is selected to avoid the backgrounds from partially reconstructed B mesons, but to include enough of the background region to determine accurately the background shape. $\mathcal{L} = \prod_{i=1}^N p_i$ is then maximized to obtain the best fit values for M_B , σ , f_s , and r_{obs} . The fitter is extensively tested with Monte Carlo samples.

The fit to 2683 candidates falling in the fitting range returns the signal fraction, $f_s = 0.736 \pm 0.012$, and the ratio of the yields of each decay mode, $r_{\text{obs}} = (4.82 \pm 0.81)\%$. These values give 1883 ± 34 signal events in the $B^\pm \rightarrow J/\psi K^\pm$ decay mode and 91 ± 15 events in the $B^\pm \rightarrow J/\psi \pi^\pm$ decay mode. The distributions in $M_{J/\psi K}$ and α for the events in the data sample are shown in Figs. 2 and 3, along with the likelihood fit results.

Possible biases in the fitting procedure are investigated by performing the fit on Monte Carlo samples generated by the PDF in Eq. (5), with known composition and with the same size as the data sample. The difference of the ratio between the extracted and the input values is consistent with zero, and the width of the pull distributions is one.

In order to determine the ratio of branching fractions, the ratio of the yields of each decay mode must be corrected with the relative reconstruction efficiency. The relative reconstruction efficiency depends in turn on the different decay in flights and nuclear interaction probabilities of the kaon and pion from the two decay modes and on the slightly different track momentum spectra. The relative reconstruction efficiency for the two decay modes is $\epsilon_{\text{rel}} = 0.991 \pm 0.005$ which is derived from the Monte Carlo simulation.

In this analysis, we use a Monte Carlo simulation to parametrize the α distributions of each signal and to de-

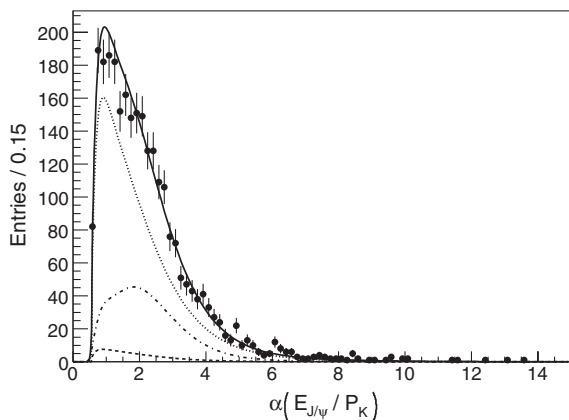


FIG. 3. The α distribution in the data sample (points) compared with the results of the likelihood fit; overall (solid line), $B^\pm \rightarrow J/\psi K^\pm$ (dotted line), $B^\pm \rightarrow J/\psi \pi^\pm$ (dashed line), and background (dash-dotted line).

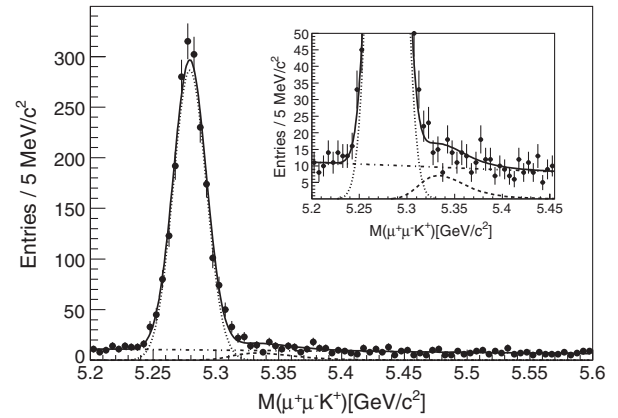


FIG. 2. The invariant mass distribution in the data sample (points) projected with the results of the likelihood fit; overall (solid line), $B^\pm \rightarrow J/\psi K^\pm$ (dotted line), $B^\pm \rightarrow J/\psi \pi^\pm$ (dashed line), and background (dash-dotted line). The inset shows the magnified region of the $B^\pm \rightarrow J/\psi \pi^\pm$ signal.

termine the relative reconstruction efficiency for the two decay modes. The Monte Carlo generation proceeds as follows. Transverse momentum and rapidity distributions of single b quarks are generated based on next-to-leading order perturbative QCD calculation [18]. B meson kinematic distributions are obtained by simulating Peterson fragmentation [19] on quark-level distributions. Additional fragmentation particles, correlated $b\bar{b}$ production, and the underlying event structure are not generated. The B meson spectrum used in the Monte Carlo simulation is from the inclusive $B \rightarrow J/\psi X$ measurement [7]. The CLEOMC program [20] is used to decay B^\pm mesons into the final states of interest. The simulation of the CDF II detector and trigger is based on a GEANT [21] description.

Since both decay modes of interest have almost identical decay topology and kinematics, most systematic uncertainties cancel in this ratio measurement, including uncertainties in total integrated luminosity and trigger and reconstruction efficiencies. Remaining systematic uncertainties come from the uncertainties in the shapes of the mass distribution, the parametrized PDFs in the α variable, and from the determination of the relative reconstruction efficiency. The largest systematic uncertainty originates from the unknown shape of the combinatorial background in the mass distribution. To estimate this effect, a second order polynomial function is considered as an alternative model for the shape of the background mass distribution. The modeling of the width of the invariant mass distribution is determined from momentum scale resolution studies [13]. An alternative model from a simple Gaussian is to include an additional Gaussian for potential different momentum resolutions of tracks reconstructed in different detector geometry coverage. We replace a Gaussian with a double Gaussian for modeling each signal mass distribution and fit again to evaluate the uncertainty coming from the non-Gaussian tails in the $B^\pm \rightarrow J/\psi K^\pm$ mass distri-

bution. The uncertainties in the function parameters describing the α PDFs, in Eqs. (3) and (4), generate an uncertainty for the ratio measurement. The contribution of this uncertainty is estimated by performing the fit by varying the parametrization variables of the PDFs by the $\pm 1\sigma$, obtained from Monte Carlo simulation. The uncertainty in ϵ_{rel} originates from the uncertainties of the nuclear interaction and the material description in the detector simulation. The GEANT simulation calculates nuclear interaction probabilities of $\approx 4\%$ for π^+ , π^- and K^- , and $\approx 3\%$ for K^+ . We then assign a 25% uncertainty to the calculated nuclear interaction probabilities as the uncertainty of the detector material description in the detector simulation and take the resulting uncertainty in ϵ_{rel} as a systematic uncertainty. We determine the total systematic uncertainty of 3.0% on the measurement by adding the individual uncertainties in quadrature, and the contributions from each source are summarized in Table I.

From Eq. (1), we derived the ratio of branching fractions,

$$\frac{\mathcal{B}(B^\pm \rightarrow J/\psi \pi^\pm)}{\mathcal{B}(B^\pm \rightarrow J/\psi K^\pm)} = (4.86 \pm 0.82(\text{stat}) \pm 0.15(\text{syst}))\%,$$

where the first error is statistical, and the second is systematic.

In conclusion, we present the measurement of the ratio of branching fractions between $B^\pm \rightarrow J/\psi \pi^\pm$ and $B^\pm \rightarrow J/\psi K^\pm$. This result is consistent with theoretical expectations and the previous measurements, and will improve the present world average ($5.3 \pm 0.4\%$) [14].

TABLE I. Summary of systematic uncertainties for the ratio of branching fractions, $\mathcal{B}(B^\pm \rightarrow J/\psi \pi^\pm)/\mathcal{B}(B^\pm \rightarrow J/\psi K^\pm)$.

Source	Uncertainty of the ratio (%)
Background shape	2.5
Non-Gaussian tail of $B^\pm \rightarrow J/\psi K^\pm$	1.2
α PDFs parametrization	1.0
Relative reconstruction efficiency	0.5
Total uncertainty	3.0

We thank the Fermilab staff and the technical staffs of the participating institutions for their vital contributions. This work was supported by the U.S. Department of Energy and the National Science Foundation; the Italian Istituto Nazionale di Fisica Nucleare; the Ministry of Education, Culture, Sports, Science and Technology of Japan; the Natural Sciences and Engineering Research Council of Canada; the National Science Council of the Republic of China; the Swiss National Science Foundation; the A.P. Sloan Foundation; the Bundesministerium für Bildung und Forschung, Germany; the Korean Science and Engineering Foundation and the Korean Research Foundation; the Particle Physics and Astronomy Research Council and the Royal Society, UK; the Russian Foundation for Basic Research; the Comisión Interministerial de Ciencia y Tecnología, Spain; in part by the European Community's Human Potential Programme under Contract No. HPRN-CT-2002-00292; and the Academy of Finland.

-
- [1] M. Wirbel, B. Stech, and M. Bauer, Z. Phys. C **29**, 637 (1985).
- [2] M. Bauer, B. Stech, and M. Wirbel, Z. Phys. C **34**, 103 (1987).
- [3] B. Aubert *et al.* (BABAR Collaboration), Phys. Rev. Lett. **92**, 241802 (2004).
- [4] K. Abe *et al.* (Belle Collaboration), Phys. Rev. D **67**, 032003 (2003).
- [5] M. Bishai *et al.* (CLEO Collaboration), Phys. Lett. B **369**, 186 (1996).
- [6] F. Abe *et al.* (CDF Collaboration), Phys. Rev. Lett. **77**, 5176 (1996).
- [7] D. Acosta *et al.* (CDF Collaboration), Phys. Rev. D **71**, 032001 (2005).
- [8] CDF II uses a cylindrical coordinate system in which ϕ is the azimuthal angle, r is the radius from the nominal beam line, and z points in the beam direction, with the origin at the center of the detector. The $r - \phi$ plane is the transverse plane perpendicular to the z axis.
- [9] A. Sill *et al.*, Nucl. Instrum. Methods Phys. Res., Sect. A **447**, 1 (2000).
- [10] T. Affolder *et al.*, Nucl. Instrum. Methods Phys. Res., Sect. A **526**, 249 (2004).
- [11] G. Ascoli *et al.*, Nucl. Instrum. Methods Phys. Res., Sect. A **268**, 33 (1988).
- [12] E.J. Thomson *et al.*, IEEE Trans. Nucl. Sci. **49**, 1063 (2002).
- [13] D. Acosta *et al.* (CDF Collaboration), Phys. Rev. Lett. **96**, 202001 (2006).
- [14] S. Eidelman *et al.* (Particle Data Group), Phys. Lett. B **592**, 1 (2004).
- [15] A. Abulencia *et al.* (CDF Collaboration), Phys. Rev. Lett. **97**, 211802 (2006).
- [16] D. Acosta *et al.* (CDF Collaboration), Phys. Rev. Lett. **94**, 122001 (2005); Abulencia *et al.* (CDF Collaboration), Phys. Rev. D **73**, 051104 (2006).
- [17] $\mathcal{M}_B^2(\alpha) = M_B^2 + (M_K^2 - M_\pi^2) + 2E_{J/\psi}(\sqrt{M_K^2 + P_K^2} - \sqrt{M_\pi^2 + P_K^2}) \approx M_B^2 + (1 + \alpha)(M_K^2 - M_\pi^2)$, assuming $p_K \gg M_K$ and $p_K \gg M_\pi$. All momentums are calculated in Lab frame.
- [18] P. Nason, S. Dawson, and R. K. Ellis, Nucl. Phys. **B303**,

607 (1988).

[19] C. Peterson, D. Schlatter, I. Schmitt, and P.M. Zerwas, *Phys. Rev. D* **27**, 105 (1983).

[20] P. Avery, K. Read, and G. Trahern, Cornell internal Report

No. CSN-212, 1985 (unpublished).

[21] R. Brun, R. Hagelberg, M. Hansroul, and J.C. Lassalle, CERN Report No. CERN-DD-78-2-REV, 1987; CERN

Report No. CERN-DD-78-2, 1987.